Fuel 338 (2023) 127234

Contents lists available at ScienceDirect

Fuel

journal homepage: www.elsevier.com/locate/fuel

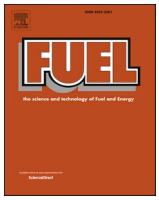

Axial segregation behaviour of a reacting biomass particle in fluidized bed reactors: experimental results and model validation

Stefano Iannello [a], Zachariah Bond [b], Alex Sebastiani [a], Matteo Errigo [a], Massimiliano Materazzi [a,*]

[a] Department of Chemical Engineering, University College London, London WC1E 7JE, UK
[b] Department of Chemical Engineering and Biotechnology, University of Cambridge, Cambridge CB3 0AS, UK

ARTICLE INFO

Keywords:
X-ray imaging
Fluidized bed
Thermal treatment
Endogenous bubbles
Biomass
Segregation

ABSTRACT

Axial segregation behaviour of a single biomass particle in a lab-scale bubbling fluidized bed has been investigated from both experimental and modelling perspectives. Experiments were conducted using beech wood particles of different sizes, ranging from 8 to 12 mm under either oxidizing or inert conditions. The fluidized bed reactor was operated at temperatures and fluidization velocity ratios, U/U_{mf}, in the range of 500–650 °C and 1–2, respectively. A one-dimensional model has been developed to predict the axial location of the particle over time, taking into account both dynamic and thermal conversion mechanisms. X-ray imaging techniques allowed to identify endogenous bubbles released during devolatilization and carry out direct measurements of their size. This information was used to propose an expression for the lift force acting on the fuel particle. The model showed very accurate predictions and the segregation behaviour of the fuel particle appeared to be independent of the nature of the fluidizing medium.

1. Introduction

Bubbling fluidized bed reactors are among the most promising technologies for the thermochemical treatment of solid feedstocks, owing to their good operational flexibility, favourable mixing features and enhanced heat and mass transfer [1–5]. In the last couple of decades, there has been a growing interest in exploiting biomass and waste as one of the possible pathways to face global warming challenges and promote the green energy transition [6,7]. Nevertheless, there are still unsolved challenges when operating with these feedstocks in fluidized bed reactors. Because of their relatively low density, these materials experience axial segregation, resulting in stratification along the bed height and poor mixing of solid and gas phases within the fluidized bed [8–13]. Moreover, the great amount of volatile matter released by the feedstock particles within the bed evolve in the form of so-called endogenous bubbles, which further enhance the segregation of the feedstock [14–18]. As a consequence of segregation, both solid and gas phases cannot take advantage of the enhanced bed-to-fuel transfer phenomena intrinsic of the fluidized-bed technology, which are essential for high product yield and quality [19,20]. All these aspects are essential to the design of industrial fluidized-bed units and relevant to all thermochemical conversion processes, since the evolution of volatiles is common to pyrolysis, gasification and combustion operations. Several researchers have carried out fundamental investigations to better understand the behaviour of a relatively large particle in bubbling fluidized beds by means of different non-invasive techniques, including PIV (Particle Image Velocimetry), X-ray, RPT (Radioactive Particle Tracking), Lagrangian sensor systems and MPT (Magnetic Particle Tracking) [14,15,21–32]. Most of these investigations have been carried out under cold conditions using tracers to resemble the behaviour of one or more moving objects, or the hydrodynamic of the bed itself. The main issue in using this approach is the lack of similarity with hot fluidized bed reactors, as the cold models do not consider the thermal decomposition of the solid fuel, which is crucial to build more comprehensive mathematical models. As demonstrated by Fiorentino et al. [15,16] and Solimene et al. [18], the volatile bubbles released by the fuel particle play a significant role, affecting the movement of the feedstock itself. In particular, the authors observed that the endogenous bubbles transfer momentum to the fuel particle and generate a lift effect that accelerates the particle itself in the upward direction. Among the diagnostic techniques cited, the X-ray imaging technique is, at present, the only one capable of providing direct visualization of flow pattern of both solid and gas phases at realistic operating conditions. As directly observed by

* Corresponding author.
E-mail address: massimiliano.materazzi.09@ucl.ac.uk (M. Materazzi).

https://doi.org/10.1016/j.fuel.2022.127234
Received 23 October 2022; Received in revised form 13 December 2022; Accepted 20 December 2022
Available online 31 December 2022

Nomenclature

Symbols

d [m]	Diameter
F [N]	Force
g [m/s^2]	Gravitational acceleration
H [m]	Height of expanded bed
k [s^{-1}]	Devolatilization rate constant
k_g [m/s]	Mass transfer coefficient of oxygen
M [kg/mol]	Molecular weight
m [kg]	Mass
P [Pa]	Pressure
Q [m^3/s]	Volumetric flow rate of volatiles
R [J/mol K]	Universal gas constant
Re [-]	Reynolds number of fuel particle
r [m]	Radius
T [K]	Temperature
t [s]	Time
U [m/s]	Gas velocity
u_e [m/s]	Interstitial velocity of emulsion gas in emulsion phase
u_{ex} [m/s]	Velocity of exogenous bubbles
y_{O2} [-]	Molar fraction of oxygen
V [m^3]	Volume
v_p [m/s]	Velocity of fuel particle
$v_p^{'}$ [m/s]	Mean rise velocity of fuel particle
w [-]	Mass composition of volatile matter in solid fuel
X [-]	Mass conversion of solid fuel
z [m]	Axial position

Greek letters

β[-]	Stoichiometric coefficient for char combustion
δ[-]	Volume fraction of bed occupied by exogenous bubbles
γ[-]	Proportional constant in Eq. (7)
ρ[kg/m^3]	Density

Subscripts

0	Detachment time of endogenous bubble
b	Endogenous bubble
c	Char of fuel particle
e	Emulsion phase
ex	Exogenous bubble
f	Fluidizing gas
i	Initial
m	Maximum
mf	Minimum fluidization
p	Fuel particle
v	Virgin core of fuel particle
vm	Volatile matter
w	Wake phase

Bruni et al. using an X-ray apparatus, at typical thermochemical conversion conditions, the endogenous bubbles are visible as long as the solid feedstock is immersed within the fluidized bed [14]. However, the conditions investigated by the authors fall within the specific regime of "single bubble segregation", meaning that one single endogenous bubble is released during the rise period of the fuel particle from the bottom to the surface of the bed. In this case, it is possible to assume that the axial displacement of the fuel particle is the same as that of the only endogenous bubble released, as asserted by the authors. This significantly simplifies the problem, whereby the behaviour of the bubble is used to describe the dynamic behaviour of the fuel particle. Although this might be advantageous from a practical perspective, in the most general case of fuel particle devolatilization, more than one endogenous bubble can be released, causing complications in developing the model. Solimene et al. quantified the bubble-induced effect under cold conditions in the form of a lift force [18], which is extremely practical to simplify such a complex phenomenon and ultimately link dynamic behaviour of the solid fuel to its thermal decomposition, as discussed in this study.

The aim of this work is to propose a simple model that can be applied to fluidized bed reactors to predict the movement, as well as the decomposition mechanism of highly volatile fuel particles during thermochemical conversion. At the same time, it was crucial to carry out experiments in order to determine the kinetics of devolatilization, validate the model and gain a better understanding of the mechanisms governing the evolution of volatiles and the decomposition of particles. This is done by using advanced imaging techniques to study the conversion of beech wood particles of different sizes in a lab-scale reactor operated at different fluidization velocities, ranging from minimum fluidization to bubbling regime.

2. Model description

2.1. Fuel particle's decomposition

A biomass particle loses its volatile content during thermochemical conversion, leaving behind char as a solid by-product. The presence of oxygen in the system (combustion/gasification condition) leads to oxidation of the char. Several authors showed that in fluidized bed reactors the fuel particle ignites following different pathways, according to the surrounding atmosphere of conversion and properties of the fuel

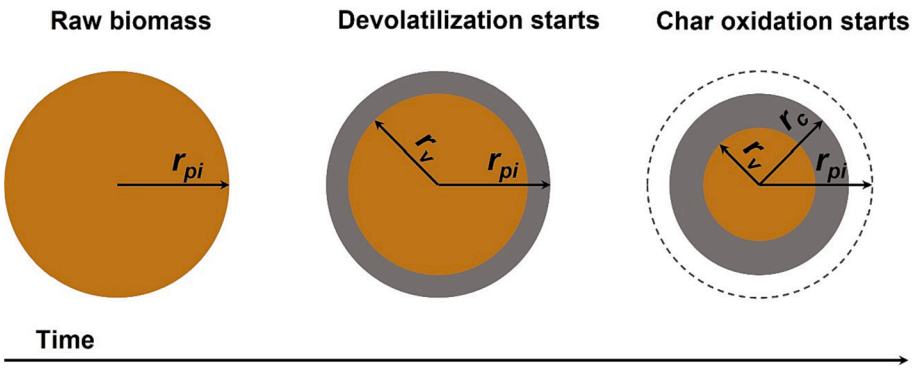

Fig. 1. Simple schematization of the conversion of a biomass particle. r_{pi}: radius of the raw biomass; r_v: radius of the shrinking biomass core; r_c: radius of the shrinking char.

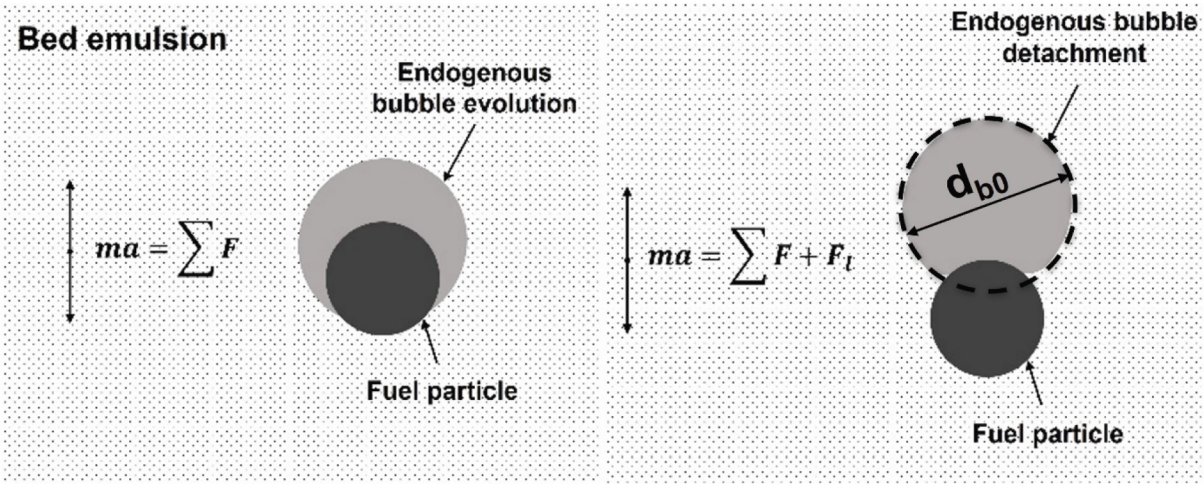

Fig. 2. Simple schematization of the evolution and detachment of an endogenous bubble, and forces acting on the fuel particle.

itself [33–35]. Bu *et al.* showed that the oxygen concentration affects the heating of the particle during the devolatilization for different types of solid fuels, including coal and wood [35]. They found that the devolatilization time decreases as the O_2 concentration increases. The authors also observed that the presence of volatile flames did not have any effect on the rate of particle heating or devolatilization time. Thus, they concluded that the oxygen reacting on the surface of the particle before the end of the devolatilization is responsible for the heating of the particle itself, and subsequent shortening of the devolatilization time. Furthermore, in a previous work it was found that the devolatilization time of beech wood particles under oxidizing conditions was shorter than that obtained under inert conditions at the same operational temperatures investigated in this work [36]. From these observations, it is reasonable to consider devolatilization and char oxidation occurring in parallel as soon as the first layer of char forms on the surface of the particle, as shown in Fig. 1.

It is assumed that devolatilization and char burnout follow a shrinking core and a shrinking particle model, respectively. The devolatilization occurs according to the following pseudo first-order rate law [16,37]:

$$\frac{dX}{dt} = k(1 - X) \tag{1}$$

It is possible to manipulate Eq. (1) to express the kinetics of devolatilization in terms of the diameter of the raw biomass, as follows:

$$\frac{dd_v}{dt} = -\frac{kd_v}{3} \tag{2}$$

Eq. (2) represents a shrinking core model, where the information about the transfer phenomena is embedded in the kinetic constant k obtained experimentally. As the first layer of char forms, the oxygen transfers from the environment to the surface of the particle, where oxidation occurs. Due to the low content of ash in biomass, under oxidizing conditions the char is consumed according to the shrinking particle model, assuming the convective mass transfer of oxygen from the emulsion to the surface of the char layer to be the controlling mechanism [38], as follows:

$$\frac{dd_c}{dt} = -\frac{2\beta k_g M_c y_{o2} \rho_f}{\rho_c M_f} \tag{3}$$

The stoichiometric coefficient β has been set equal to 2, according to the reaction of char oxidation:

$$2C + O_2 = 2CO \tag{4}$$

As evidenced in the literature, in the range of temperatures investigated in this study the oxidation of CO to CO_2 is inhibited in the proximity of the burning char because of the sand surrounding the particle, which provides enough surface area for radicals to recombine. As a consequence, the CO_2 forms mostly in the homogenous gas phase, after the CO diffuses away from the particle [39,40].

2.2. Fuel particle's motion

The fuel particle interacts with the fluidized bed and its motion can be described by a force balance. It is important, however, to distinguish between minimum fluidization and bubbling regimes to define the proper equation of motion. At minimum fluidization, the fluidized bed is considered as a homogeneous and continuous medium (the emulsion phase) with a bulk density ρ_e. In this case, the force balance is given by the following equation:

$$\rho_p V_p \frac{d^2 z_p}{dt^2} + F_a = F_g + F_b + F_d + F_l \tag{5}$$

The added mass force F_a is induced by the displaced mass of fluidized bed surrounding the moving fuel particle, which accelerates (or decelerates) the particle itself. F_l is the lift force associated with the rise of endogenous bubbles, which is always directed upwards. A schematization of the endogenous bubbles' evolution and detachment is shown in Fig. 2.

It is assumed that each endogenous bubble released transfers momentum to the fuel particle as it detaches from the particle itself [18], meaning that the lift force acts on the fuel in an intermittent fashion. The devolatilization rate increases with temperature, resulting in larger bubbles released from the fuel particle. The observed phenomenon was assumed to be the same as the formation of a bubble from an orifice in a bed at minimum fluidization [18]. Therefore, the time of formation (or detachment time) for a single bubble can be described by the following equation:

$$t_0 = \frac{V_{b0}}{Q} \tag{6}$$

However, several authors noted that the visible bubble flow through the orifice accounted only for a fraction of the total gas injected into the bed [41]. Thus, Eq. (6) can be corrected as follows:

$$t_0 = \gamma \frac{V_{b0}}{Q} \tag{7}$$

where γ is related to the ratio between visible bubble flow and the actual flow of volatiles released by the particle [42]. The bubble can be considered as fully formed when the displacement is equal to its radius,

Table 1
Mathematical expressions of the forces used in the model at U_{mf}.

Name	Equation	
Gravitational force	$F_g = -\frac{\pi}{6}\rho_p d_c^3 g$	(12)
Buoyancy force	$F_b = \frac{\pi}{6}\rho_e d_c^3 g$	(13)
Drag force	$F_d = \frac{\pi}{8}\rho_e C_D d_c^2 (u_e - v_p)\lvert u_e - v_p\rvert$	(14)
Drag coefficient [32]	$C_D = \frac{24}{\mathrm{Re}}(1 + 0.15\mathrm{Re}^{0.687})$	(15)
Added mass force	$F_{a,mf} = \frac{\pi}{12}\rho_e d_c^3 \frac{\mathrm{d}^2 z_p}{\mathrm{d}t^2}$	(16)
Lift force	$F_l = 0.506\gamma^{1.2}\rho_e g^{0.4} Q^{1.2}$	(17)

as given by the following equation [43]:

$$g t_0^2 = d_{b0} \tag{8}$$

Endogenous bubbles were assumed to be spherical and the equivalent circle, as shown in Fig. 2, represents the cross-sectional area of the bubble itself. Solutions of Eqs. (7) and (8) lead to:

$$d_{b0} = 1.259\gamma^{0.4}\frac{Q^{0.4}}{g^{0.2}} \tag{9}$$

The volumetric volatile flow rate can be expressed by the following first-order rate law:

$$Q = \frac{m_{pi} w}{\rho_{vm}}\frac{\mathrm{d}X}{\mathrm{d}t} = \frac{m_{pi} w}{\rho_{vm}} k e^{-kt} \tag{10}$$

After manipulation of Eqs. (9) and (10), the bubble diameter at the detachment time becomes:

$$d_{b0} = 1.259\frac{\gamma^{0.4}}{g^{0.2}}\left(\frac{\pi k \rho_{pi} w R T}{6 P M_{vm}}\right)^{0.4} d_{pi}^{1.2} \tag{11}$$

Endogenous bubbles are produced as long as the fuel particle is immersed within the bed. In the case of highly volatile feedstocks, such as biomass, the residence time of the fuel particle within the bed is much shorter than the whole devolatilization time [2]. Therefore, the term e^{-kt} does not appear in Eq. (11), as it approaches to unity. It is important to note that the above discussion is valid as long as the residence time of the fuel particle within the bed is much shorter than the whole devolatilization time. This condition is usually met in the case of highly volatile feedstocks in bubbling fluidized beds [2]. Table 1 shows the equations for the main forces used in the model. Further details about the lift force are discussed in Section 4.

In the more complex case of bubbling fluidization regime, the bed is assumed to behave according to the 2-phase theory [44,45]. As observed by Rowe and Nienow, the upward movement of solid particles in a bubbling fluidized bed is associated with that of the wake of rising bubbles [46]. Therefore, it is assumed here that the fuel particle's upward motion takes place within the wake region of the bubble phase, which moves upward at the velocity of the rising exogenous bubbles. With the term exogenous bubble, we indicate the bubbles typically observed in a bubbling regime, when the velocity of the fluidizing agent is higher than the minimum fluidization velocity. The physical properties of the bubble wake are assumed to be the same as for the emulsion phase. In this case, the interstitial velocity of the emulsion gas u_e in Eq. 14 is substituted by the rising velocity of the exogenous bubbles u_{ex}, given by the following equations [44]:

$$u_{ex} = \left(U - U_{mf}\right) + 0.711(g d_{ex})^{0.5} \tag{18}$$

$$d_{ex} = d_{ex,m} - \left(d_{ex,m} - d_{ex,i}\right)e^{-0.3z/d_{bed}} \tag{19}$$

In the bubbling regime, it is also necessary to modify the equation of the added mass force (Eq. 16), as follows:

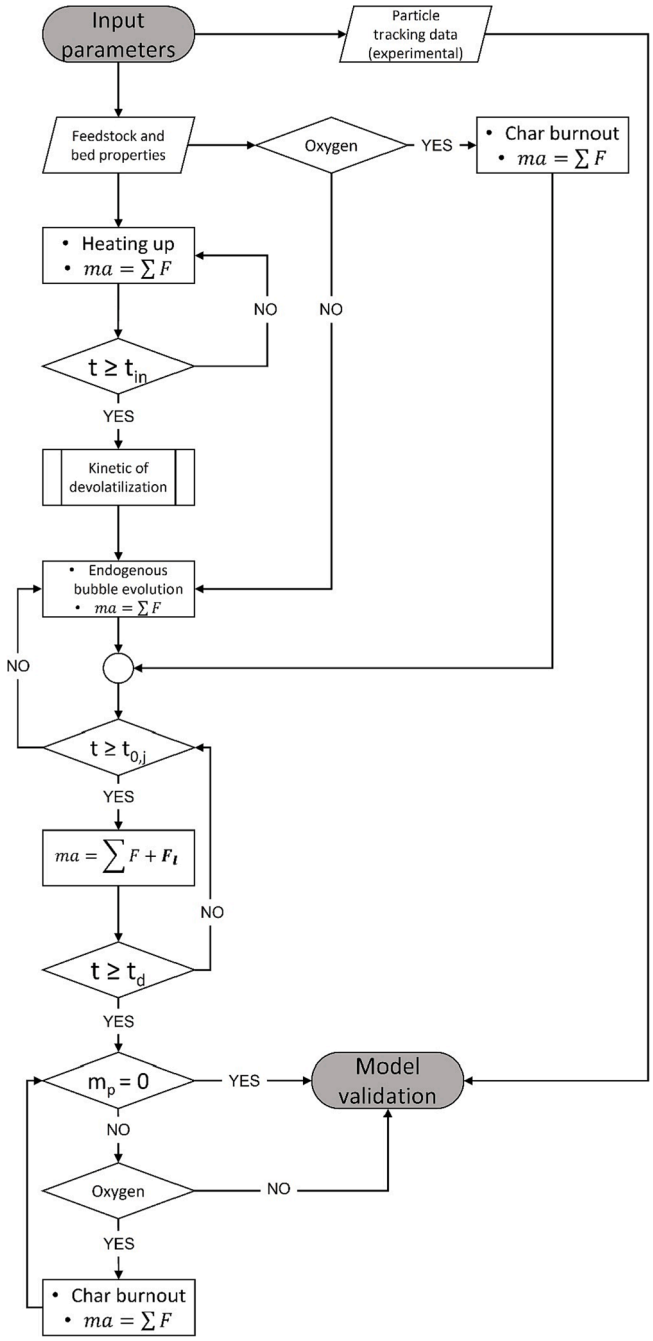

Fig. 3. Computational routine of the model.

$$F_{a,w} = \frac{\pi}{12}\rho_e d_c^3\left(\frac{\mathrm{d}^2 z_p}{\mathrm{d}t^2} - u_{ex}\frac{\mathrm{d}u_{ex}}{\mathrm{d}z}\right) \tag{20}$$

The additional term in Eq. (20) arises from the fact that the particle is moving within a non-uniform velocity field, which, according to the 2-phase theory, varies along the height of the bed. This is not true at minimum fluidization, as the emulsion gas velocity is uniform along the entire fluidized bed.

The model has been implemented in MATLAB® software and the computational routine is shown in Fig. 3.

The computation starts as the particle is fed into the bed. After an initial period of heating up t_{in}, the first endogenous bubble starts forming (beginning of devolatilization) and it detaches from the fuel particle at the instant of time $t_{0,1}$, when the lift force acts on the particle. At this point, a second endogenous bubble starts evolving until the detachment

Table 2
Materials and experimental conditions used.

Fuel particle			
Material	d_{pi} (mm)	Density of raw sample (kg/m^3)	Range of densities with lead tracer (kg/m^3)
Beech wood	8, 10, 12	774 ± 0.012	804 – 1157
Bed inventory			
Material	Geldart classification	Particle density (kg/m^3)	Average particle size (μm)
Quartz sand	B	2650	250
Bed operating conditions			
T (°C)	U_{mf} (mm/s)		
500	34.8		
600	30.5		
650	27.9		

Table 3
Typical physical and chemical properties of beech wood.

Ref.	[47]	[48]	[49]
Ultimate analysis, (wt%)	db	daf	db
C	48.1	49.2	49.1
H	5.9	6.0	5.7
O	45.4	44.1	44.5
N	0.2	0.5	0.15
S	–	0.02	0.045
Proximate analysis, (wt%)	wb	db	db
Volatiles	74.8	85.3	84.3
Fixed carbon	15.7	14.3	15.2
Ash	0.7	0.4	0.5
Moisture	8.8	0	8.7^{ar}
Heating value db, [MJ/kg]	15.0	–	–

ar: as received, daf: dry ash free, db: dry basis, wb: wet basis

time $t_{0,2}$ and so forth until the end of the devolatilization period. The induction time varies between 0.3 % and 0.7 % of the entire devolatilization period, according to temperature and initial size of the biomass particle [36]. The kinetics of devolatilization have been determined experimentally through gas measurements at the conditions investigated. The char burnout starts if oxygen is present in the system and after the fuel particle shows the first layer of char on its periphery. The numerical integration proceeds with a varying timestep, which changes during the computation according to the elapsed time between two consecutive endogenous bubbles. The computation stops when the particle is completely consumed (oxidizing conditions) or when the devolatilization ends (inert conditions).

3. Methodology

3.1. Materials

Experiments were carried out using spherical beech wood particles with 3 different diameters (8, 10 and 12 mm), under either oxidizing (air) or inert (nitrogen) conditions, in order to assess the effect of the nature of the fluidizing medium on the thermal decomposition and dynamic behaviour of the fuel particle. All the samples were half-drilled in order to insert a small tracer particle of lead, ranging from 1.5 to 2 mm in diameter, to make the particle visible upon X-ray exposure during the experiments. The fluidized bed reactor consisted of a 146 mm ID × 1000 mm long Inconel cylindrical vessel operated at temperatures of 500, 600 and 650 °C, and U/U_{mf} ratios between 1 and 2. Experiments at minimum fluidization enabled the assessment of endogenous bubbles evolution without possibilities of confusion arising from exogenous bubbles. Measurements of the bubble size provided a better understanding concerning the evolution of volatiles within the bed under real thermochemical conversion conditions. On the other hand, the bubbling regime was investigated up to $2U_{mf}$ in order to avoid turbulent or slugging conditions, when the more vigorous motion of both solids and gases might cause further complications in describing the phenomena. The possible interactions between exogenous and endogenous bubbles, such as coalescence, have not been assessed in this study.

The reactor was fitted with a purposely designed single fuel particle injector, consisting of a 28 cm piston rod enclosed in a 50 cm stainless steel tube and operated by a pneumatic actuator into the reactor. At rest, the piston is retracted to allow the placement of the biomass particle into the tube through a threaded hole, which is then closed with a bolt to isolate the entire system from the environment. Consequently, nitrogen is fed through the tube to remove residual air and prevent heating and reaction before the fuel particle injection. During each experimental test, a single particle of biomass was fed into the bottom of the bed, 2.5 cm above the distributor plate. The bed height varied in the range of 16 – 18 cm, according to the conditions used. The materials and experimental conditions used are summarized in Table 2. Values of U_{mf} at the different temperatures investigated have been determined experimentally by pressure drop measurements. Typical physical and chemical properties of the biomass investigated are listed in Table 3.

A range of particle densities from 804 to 1157 kg/m^3 has been tested in order to investigate the behaviour of a reacting biomass particle after injection into a fluidized bed. The lowest range of 804 – 900 kg/m^3 resembles the density pure beech wood [50]. The highest range of 979 – 1157 kg/m^3 was investigated to expand the range of application of the proposed model, since the high densities chosen lie in the range of pelletized solid feedstock [51,52].

In order to measure the devolatilization and char burnout time, different gas sensors have been arranged in parallel, in order for the product gas to flow in each sensor at the same time. This allows to measure all the gas species simultaneously, avoiding significant delay time for the gas stream to flow from one measurement chamber to the other. A GSS SprintIR-WF-20® was used to measure changes in CO_2 concentration in the gas stream at the outlet of the reactor, whilst two CO2METER® sensors were used to detect CO and CH_4. The data collected from the gas analysis have been deconvoluted, taking into account the delay time and time constant of the system, which have been quantified by measuring the response of the system to a step of a tracer gas (CO_2) injected at the surface of the fluidized bed (location where the particle is most likely to settle during the conversion). Injecting the tracer gas at the surface of the bed is a reasonable choice, since the segregation time of the fuel particle is generally much lower than the whole thermal decomposition time and the release of the volatile content, as well as the pyrolysis and oxidation reactions, mostly take place within the freeboard of the reactor. The dynamic of the fluidized bed and sampling lines was described with a first-order time constant and pure delay time in the range of 4.7 – 10 s and 8.5 – 12.4 s, respectively. These values depend on the temperature and fluidization velocities used, as they affect the dynamics of the system.

3.2. X-ray imaging technique

A non-intrusive X-ray imaging technique used in this study provides both online visualization and image acquisition with time and spatial resolutions of 36 frames per second and 0.17 mm/pixel, respectively. Fig. 4 shows a schematization of the apparatus.

A high-energy X-ray beam passes through the fluidized bed where absorption occurs, depending on the distribution and amount of solids and fluids along the beam path. A high-speed video camera is synchronised to the beam to monitor rapid changes in the internal flow patterns associated with motion and bubble formation. The main elements of the equipment are the X-ray source and the image intensifier. The voltage is applied to the X-ray generator, which gives the penetrating power to the X-rays produced. Increasing the voltage shortens

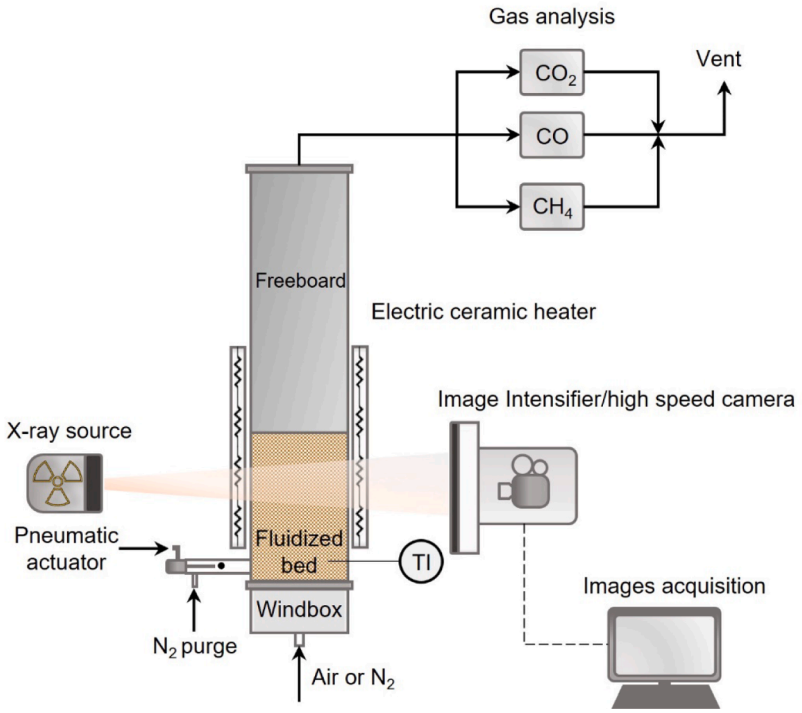

Fig. 4. Schematic representation of the experimental set-up.

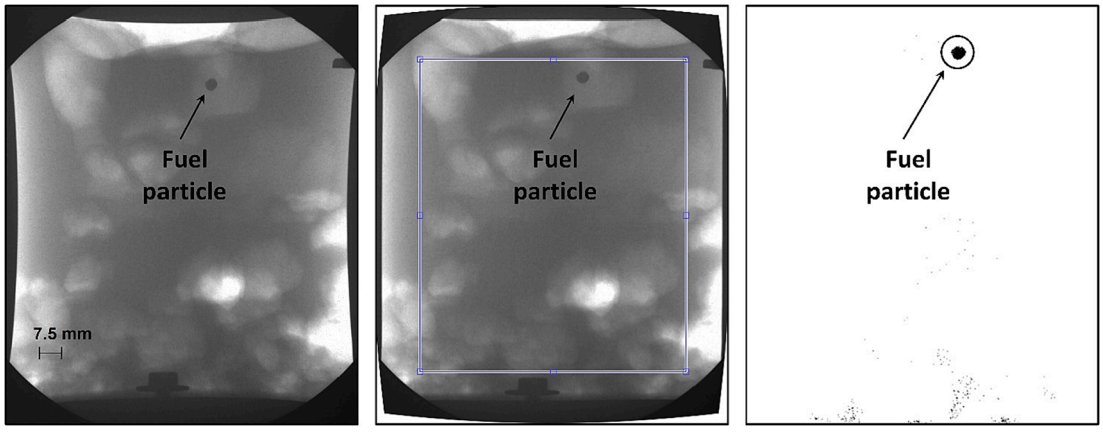

Fig. 5. Main steps of the X-ray image analysis. From left to right: raw image, correction of pincushion distortion and selection of ROI, particle tracking and final post-processed image.

the boundary of the wavelength and increases the beam intensity, whilst the current level controls the radiation intensity. In the present work, values of 135 kV and 300 mA have been used for voltage and current, respectively. Furthermore, it is possible to control the radiation produced for the X-ray pulse, and therefore the brightness of the video image. The duration of each X-ray pulse is kept as short as possible (1 ms) to ensure a sharp X-ray picture and to minimize the heat generated by the instrument.

Different algorithms have been developed in the MATLAB® environment in order to post-process the images acquired. The main steps to be considered for the post-processing stage are [36,42,53]:

- The correction of pincushion distortion due to the intrinsic curvature of the image intensifier and diverging nature of the X-ray beam.
- Filtering, contrast adjustment, image segmentation and selection of the region of interest (ROI), i.e., a specific area of the image. In the present case, this is done to remove any source of noise that may disrupt the particle tracking and is not useful to the analysis, such as the freeboard, and focus the attention on the fluidized bed, endogenous bubbles and fuel particle only.
- Particle tracking to determine the particle trajectory, hence information about the axial segregation behaviour of the fuel particle.

The main steps of the image processing and analysis are shown in Fig. 5.

Knowledge of the size of endogenous bubbles, gained by direct visualization from the collected X-ray images, allowed an estimation of the lift effect acting on the reacting particle, which was implemented in the model developed.

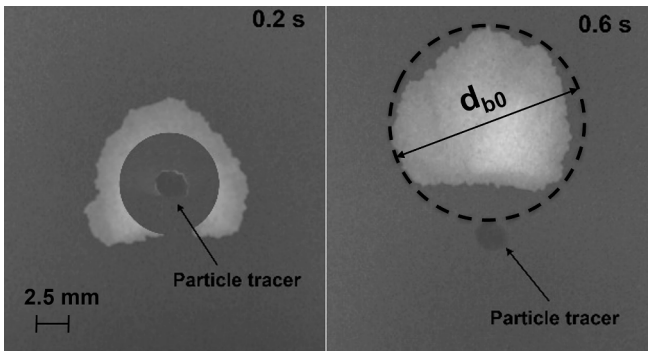

Fig. 6. Post-processed X-ray frames showing evolution and detachment of an endogenous bubble, and measurement of the equivalent bubble diameter at the detachment time for a 12 mm particle at 650 °C.

Table 4
Devolatilization rate constants and parameter γ obtained at different operating conditions. Values of d_{b0} and k were obtained experimentally. Values of γ were obtained by linear regression using Eq. (11).

T (°C)	d_{pi} (mm)	d_{b0} (mm)	$k \cdot 10^2$ (s^{-1})	γ
500	8	5.16	2.31	1.47
	10	6.85	1.85	
	12	8.64	1.55	
600	8	10.1	2.79	5.27
	10	13.6	2.24	
	12	15.1	1.87	
650	8	10.5	3.02	5.14
	10	14.3	2.42	
	12	15.7	2.03	

4. Results and discussion

4.1. Induced endogenous bubble lift effect

An X-ray visualization of evolution and detachment of an endogenous bubble from the biomass particle is shown in Fig. 6.

The X-ray schematization in Fig. 6 was obtained through post-processing of two collected images for ease of visualization, where the fuel particle (lead tracer) and a single endogenous bubble have been isolated from the rest of the background. This was done in order to represent the mechanism of devolatilization without confusion arising from secondary volatile streams produced by the particle in the other spatial directions.

In order to obtain quantitative information about the lift effect induced by the endogenous bubbles on the fuel particle, a linear regression has been performed using Eq. (11). In this way, it was possible to determine the parameter γ at each temperature considered. Results are reported in Table 4. Three repetitions have been performed per each set of conditions, and from 9 to 19 endogenous bubbles could be measured during each experiment.

Kinetic constants k and endogenous bubbles size were obtained in a previous work from gas analysis and X-ray measurements, respectively [36]. Values of k in inert fluidizing gas have been used for the fitting procedure, since it was found that the nature of the fluidizing medium does not affect the evolution of endogenous bubbles within the bed [36]. Values of d_{b0} calculated with Eq. (11) are in good agreement with the experimental observations ($R^2 = 0.88$). It was observed that the fuel particle follows a multiple bubble segregation pattern. Thus, measurements of d_{b0} were averaged along the residence time of the particle within the bed for each test. Solimene *et al.* [18] derived a correlation for the lift force, assuming that the diameter of the endogenous bubbles at the detachment time is equal to the diameter of the fuel particle. However, experimental evidence from this work (obtained with particles smaller than those used in [18]) does not support this assumption and suggests that the endogenous bubble size is highly sensitive to the bed temperature. This dependence is included in the fitting parameter γ, which has been used to propose a revised version of the lift force (Eq. 17).

4.2. Axial segregation of the biomass particle

Fig. 7 shows experimental and calculated particle segregation profiles of a single biomass particle at different fluidization regimes. The values of 0 and 1 on the y-axis correspond to the dimensionless feeding point and surface of the bed, respectively.

The model is in good agreement with the experimental observations under both minimum and bubbling fluidization regimes, up to $2U_{mf}$. There is no significant difference between the experimental axial trajectories of the particle under oxidizing and inert fluidizing conditions. This finding further confirms that the oxidizing nature of the fluidizing gas does not affect the properties of the endogenous bubbles, hence the magnitude of the lift force. The lack of interaction between bubbles and bed emulsion was also observed by Dennis et al., who studied the ignition behaviour of propane/air mixtures in fluidized bed [54]. They noticed that below 800 °C the conversion of the mixture was confined to the freeboard, where the bubbles erupt, indicating that the combustion

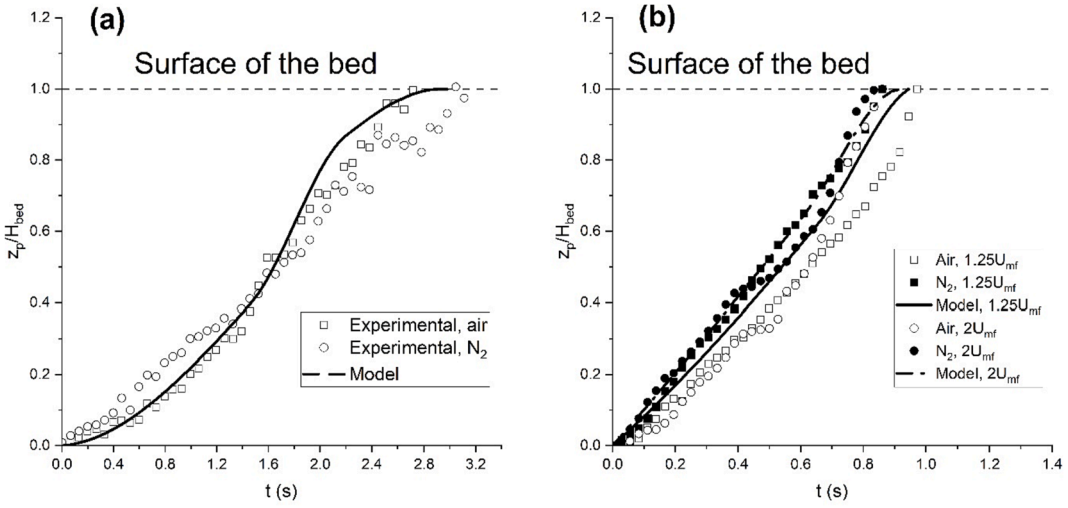

Fig. 7. Axial segregation profiles of a beech wood particle (900 kg/m^3) during devolatilization at (a) minimum fluidization and (b) bubbling regime.

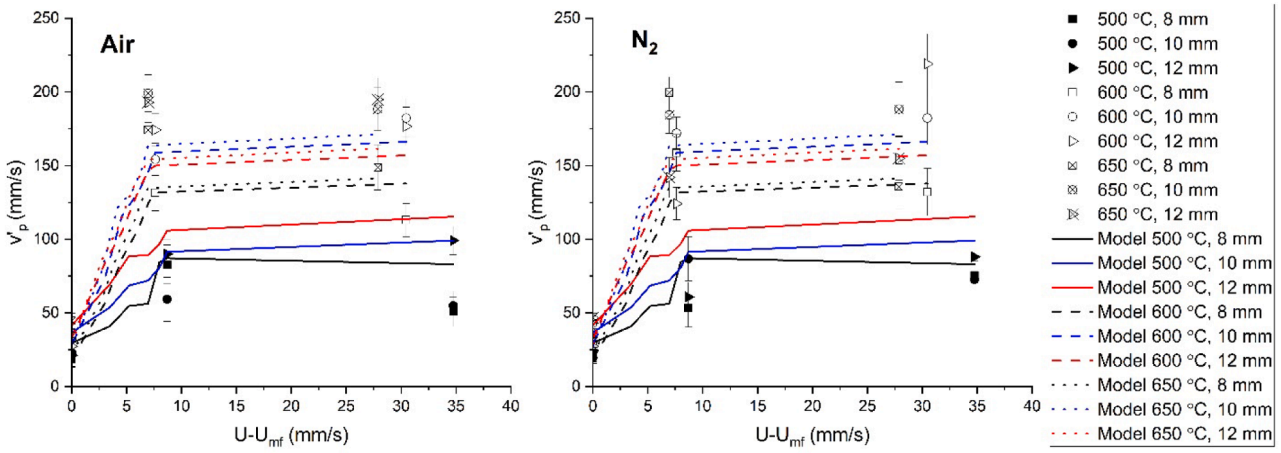

Fig. 8. Mean rise velocity of fuel particle (900 kg/m^3) *vs* excess fluidization velocity.

takes place in a homogeneous gas phase. The authors also observed that, even at 850 °C, the bubbles ignited higher up in the bed as the air-to-fuel ratio decreased. This suggests that the bubbles bypass might be further enhanced in a bubbling fluidized bed in the case of gasification (partial oxidation conditions). Similar results were also found by other researchers [55–57]. It is important to note that the studies mentioned refer to air and combustible gas that are pre-mixed before the injection into the bed at high temperature. In the present case, the in-bed ignition of volatiles released by the biomass particle may be further delayed since the oxygen must transfer from the emulsion to the bubble phase in order for oxidation to occur [36].

Fig. 8 shows the average rise velocity of the fuel particle against the excess fluidization velocity.

The particle velocity does not significantly depend on the bed temperature at minimum fluidization. However, as the bed starts bubbling, the rise velocity shows an increase, which is more evident at 600 °C and 650 °C. At these two temperatures, the more vigorous release of volatiles from the particle produces larger endogenous bubbles, as predicted by Eq. (11). At 600 and 650 °C, the mean rise velocity of the fuel particle in bubbling regime is between 4 and 5 times greater than that measured at minimum fluidization. Several authors observed that a fuel particle in a bed at ambient temperature segregates slower than a reacting one under thermal conversion conditions due to the presence of endogenous bubbles [2,14,17,18]. Rees *et al.* [58] investigated the behaviour of a buoyant sphere in a bubbling bed at room temperature and found that its mean rise velocity increased with the excess gas velocity between 5 and 20 mm/s for a sphere of 9 mm diameter and 900 kg/m^3 and similar hydrodynamic conditions as those used in this work. Fig. 8 also shows that the rise velocity of the biomass particle varies in the range of 19–219 mm/s, which is much higher than that found in [58], confirming the great influence of endogenous bubbles on the dynamic behaviour of the fuel particle. Furthermore, Rees *et al.* [17] found that the time of rise of different types of feedstock is independent of the fuel size at temperatures between 700 and 900 °C. Although the authors investigated the phenomenon in slugging regime, a similar behaviour can be observed in the bubbling regime and temperature range used in this study (Fig. 8). There is no significant difference between fuel particle rise velocities obtained under inert and oxidizing conditions. This further confirms that the magnitude of the lift force is not significantly affected by the fluidizing gas used and the endogenous bubbles tend to bypass the solids of the bed and react in the freeboard of the reactor [2].

4.3. Particle conversion and behaviour at the bed surface/splash zone

In this section, we attempt to describe the behaviour of the biomass particle at the surface of the bed, and the link between segregation and

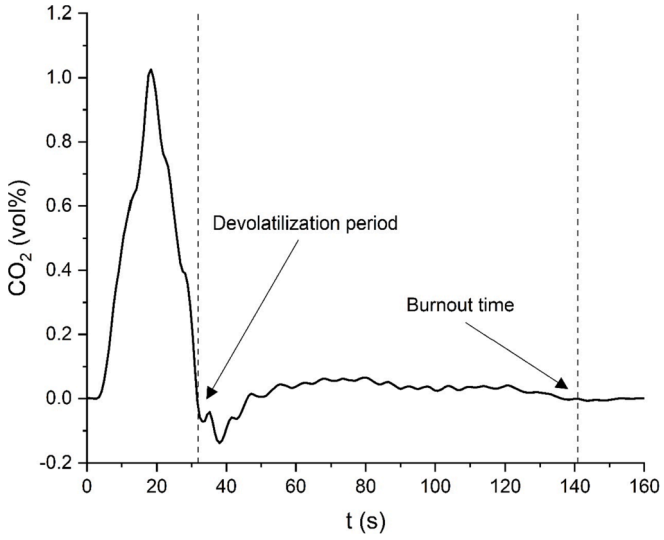

Fig. 9. Deconvoluted concentration profile of CO_2 during oxidation of an 8 mm beech wood particle at 600 °C and minimum fluidization velocity.

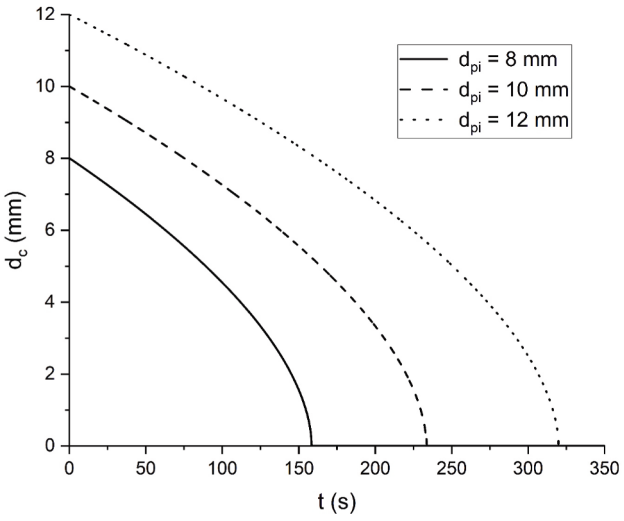

Fig. 10. Predicted change of biomass particle diameter as a function of time at 600 °C.

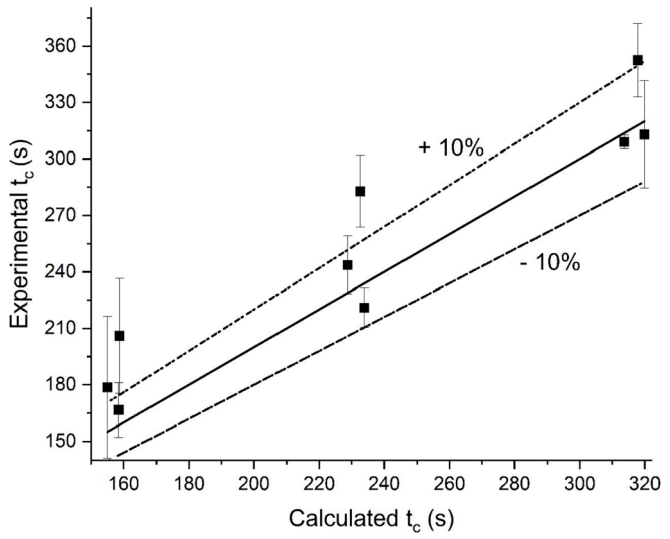

Fig. 11. Predictive capabilities of the shrinking particle model.

particle conversion during oxidation experiments. Fig. 9 shows the CO_2 concentration profile during a combustion test. The effect of the deconvolution can be observed from the graph, as the curve goes below zero. This depends on the magnitude of the response time of the system. Large response times correspond to greater undershoots.

As also observed by several researchers, the curve can be seen as the composition of two different curves. The first one is associated with the devolatilization time, which was used to develop the kinetics of devolatilization and obtain values for k in Eq. (2), while the second curve corresponds to the burnout of the residual char [17,59].

Fig. 10 shows the change of the particle's diameter over time, as predicted by the shrinking particle model (Eq. (3)). Graphs for the other operating temperatures investigated are not reported to avoid redundancy, as the trends appear to be similar.

The particle size decreases over time due to the reaction with oxygen. The slope increases as the initial fuel particle's size decreases. From these graphs, it is possible to determine the predicted time of char burnout (or complete particle conversion) as the time needed for the particle size to reach zero. Fig. 11 shows the predictive capability of the shrinking particle model. The error bars represent the standard deviation calculated from 6 observations at each initial particle size and temperature tested.

The experimental particles' burnout time varied between 167 and 353 s, depending on initial size and operating temperature. Generally, the experimental points are in good agreement with the calculated values. However, a great variability can be observed for some of the values. These differences can be attributed to the fragmentation and comminution mechanisms, i.e., continuous change in particles size and shape, which typically occurs during thermochemical conversions in fluidized bed reactors [45,60,61]. As a consequence, the burnout time is affected. Furthermore, in the present case the particle breakage may be further promoted by the presence of the hole in the samples, which introduces a fragility in the material.

The overall density of the fuel particle changes over time, owing to the loss of volatile matter, the shrinking of char and the presence of a lead tracer inside the particle. Because of the assumptions of progressive shrinking model made previously, the particle density can be assumed to vary according to the following equation:

$$\rho_p(t) = \frac{\rho_v d_v^3 + \rho_c (d_c^3 - d_v^3) + 6m_l/\pi}{d_c^3} \tag{21}$$

Fig. 12 shows experimental and predicted axial segregation profiles

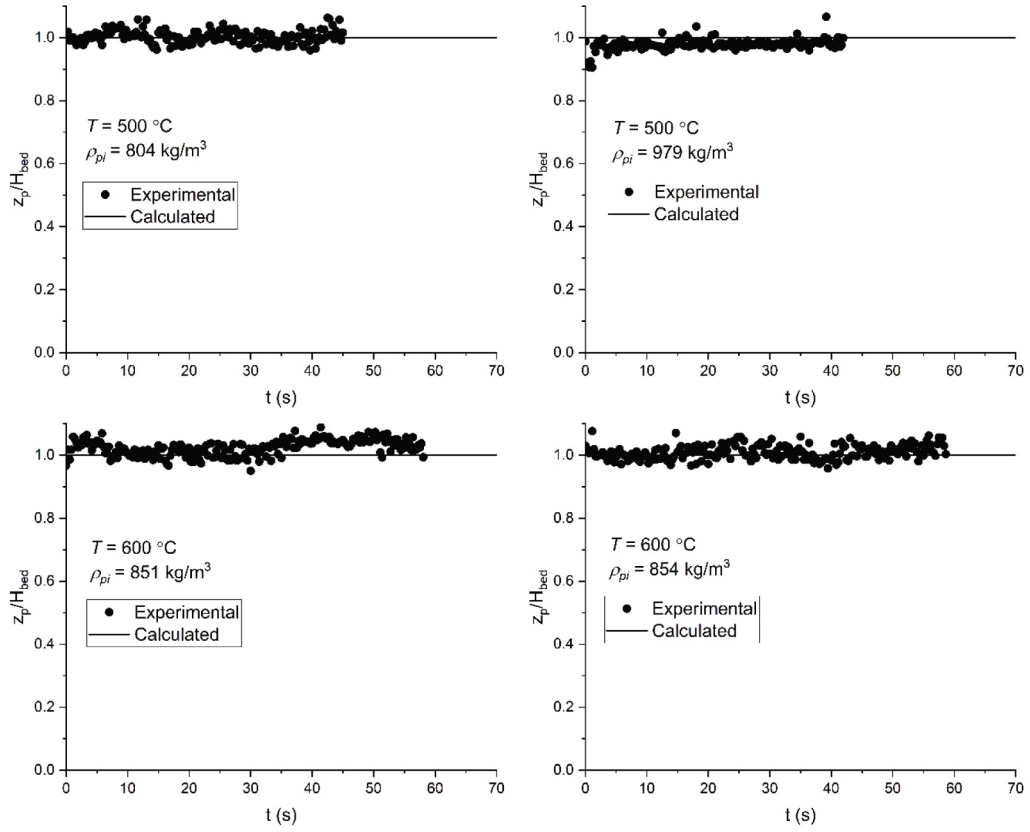

Fig. 12. Experimental and predicted locations within the fluidized bed for different particle densities at $2U_{mf}$.

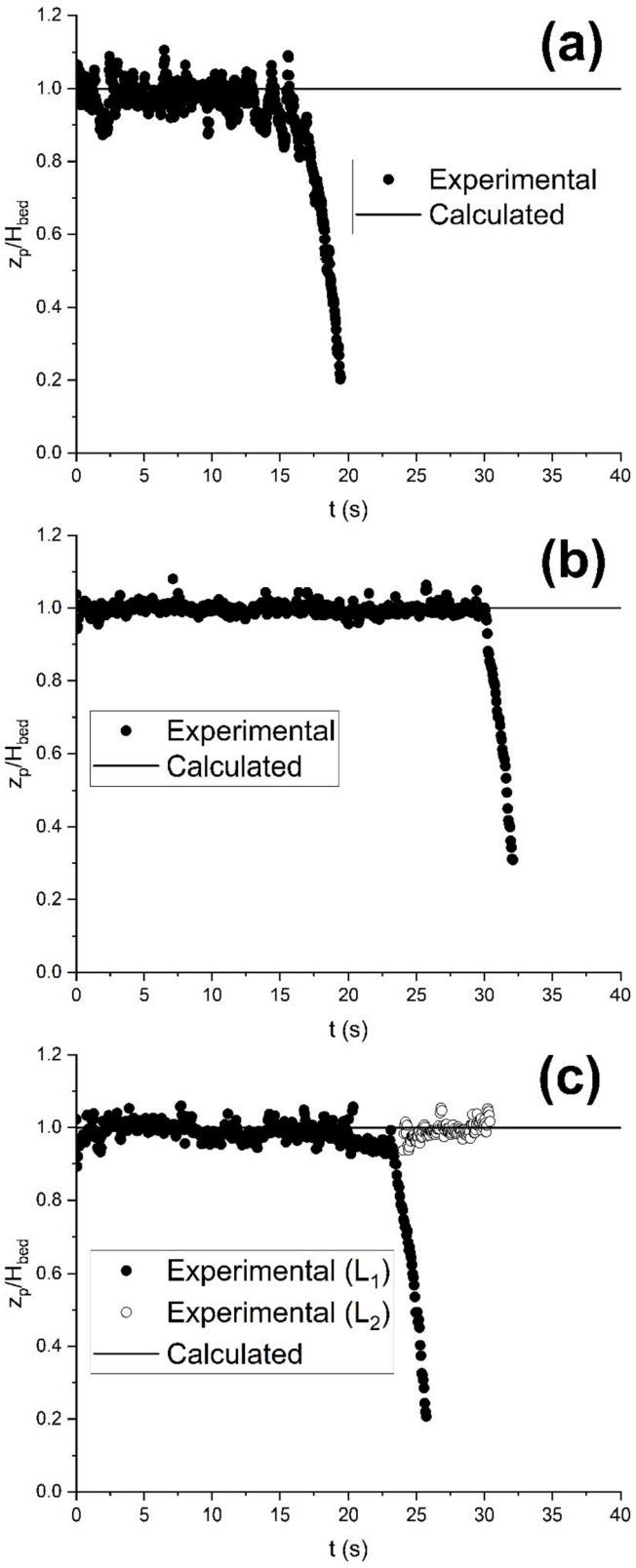

Fig. 13. Experimental and predicted axial segregation profiles for the heaviest biomass particles investigated at 600 °C and $2U_{mf}$. (a) ρ_{pi} = 1012 kg/m^3; (b) ρ_{pi} = 1151 kg/m^3; (c) ρ_{pi} = 1157 kg/m^3.

for other particle densities investigated.

The biomass particle settled at the surface of the bed for the entire time of observation, regardless the change of density occurred during its decomposition. The model developed is in good agreement with the experimental results. However, a different behaviour can be observed for the heaviest particles investigated, as shown in Fig. 13.

For the initial particle density of 1012 kg/m^3 (Fig. 13-a), it was observed that the experimental axial profile presents many fluctuations when the fuel particle is at the surface/splash region of the bed. In this case, the particle was also found either above (splash zone) or slightly underneath the surface. This is due to the eruption of exogenous bubbles at the bed surface, which generates a more vigorous motion than that observed when the particle is fully immersed within the bed, starting from about 17 s of operation. On the other hand, for the larger densities of 1151 and 1157 kg/m^3, the same behaviour is not observed, as they are less likely to be dragged up to the splash zone and tend to remain relatively still at the surface of the bed. In all cases, the particle started segregating towards the bottom of the bed after about 20 – 30 s from the feeding instant. The model appears to fail in predicting the time at which the fuel particle sinks. However, an interesting behaviour can be observed for the largest particle density in Fig. 13-c. At about 25 s from the start of the experiment, the lead tracer broke into two pieces and one of them was bigger than the other. As a result, it was possible to track the two different tracers, one of which sank (largest piece, L_1), whilst the other one kept floating on the surface of the bed (smallest piece, L_2). A possible reason to explain this behaviour is that the lead tracer used to make this high-density sample was relatively larger than the other tracers and it was highly deformed when pushed into the sample. This might have generated mechanical stress and weak regions within the structure of the tracer which, with the help of the high operational temperature, softened and separated. It is likely that the splitting of the lead was possible to observe because the fuel particle was not able to hold the tracer together as a result of its shrinkage and breakage during the operation. On the other hand, the biomass and char fragments probably remained at the bed surface due to their relatively low density. From this observation it is not possible to conclude that the sinking observed in Fig. 13-a and Fig. 13-b was caused by an increase of the density of the fuel particle over time, but it might be a consequence of the breakage of the fuel particles which lost the lead tracer within. It is important to remind that the X-ray technique used in this study does not allow to visualize the biomass particles, but only the lead tracers, due to the high attenuation of the X-ray beam provided by this material. These observations support the discrepancies discussed previously about the time of burnout of the biomass particle (Fig. 11). Nevertheless, further investigation is required to implement phenomena of particle breakage/fragmentation in the model to improve the accuracy of the predictions. This might be particularly important when many fuel particles are present within the fluidized bed, where the fragmentation can be even more likely to occur, owing to the multiple collisions that the particles can experience.

5. Conclusions

The behaviour of a reacting biomass particle in a fluidized bed has been investigated from both experimental and modelling perspectives. Advanced X-ray imaging techniques were used to investigate the release of volatiles from a single biomass particle and its interaction with a fluidized bed either during pure pyrolysis or under oxidizing conditions. Experimental results showed that the oxidizing nature of the fluidizing medium does not significantly affect the endogenous bubbles' properties, as well as the motion of the fuel particle itself within the fluidized bed. Volatiles burn when they are well mixed with the fluidizing gas in the emulsion phase, so that the production of volatiles and of endogenous bubbles is only slightly affected by the presence of oxygen in the fluidizing agent, as observed by other researchers. Measurements of the size of endogenous bubbles obtained from X-ray images at minimum

fluidization were used to quantify the lift effect acting on the fuel particle. The one-dimensional mathematical model showed accurate predictive capabilities for both minimum and bubbling fluidization conditions. At these temperatures, the mean rise velocity of the fuel particle in bubbling regime is about 4 times greater than that measured at minimum fluidization. Particle burnout time measured under oxidizing conditions is in good agreement with the predicted values obtained from a shrinking particle model, ranging from 167 to 353 s, depending on initial particle size and operating temperature. Slightly large standard deviations observed for some conditions might be associated with comminution and fragmentation phenomena that particles experience during decomposition, which cause changes in both shape and size. These phenomena could be clearly observed during the experiments with the high-density particles. In all cases, it was possible to observe that the heavy lead tracer sank between 20 and 30 s from the beginning of the experiment. This behaviour was attributed to the breakage of the fuel particle.

Further investigation is needed to better understand the effect of exogenous bubbles and their interaction with volatile matter on the behaviour of feedstock particles in fluidized beds, as well as the effect and frequency of fragmentation of the fuel particles. This may need the development of different diagnostic techniques since the two-dimensional grey scale images collected with the X-ray facility do not allow to distinguish between endogenous and exogenous bubbles, and to visualize fragments of feedstock particles after breakage. Improving the level of detail and knowledge of these phenomena may help to improve existing models and promote the development of new predictive techniques to aid the exploitation of fluidized beds in the field of thermochemical conversion of solid feedstocks.

CRediT authorship contribution statement

Stefano Iannello: Conceptualization, Methodology, Formal analysis, Investigation, Writing – original draft. **Zachariah Bond:** Conceptualization, Methodology, Investigation, Writing – review & editing. **Alex Sebastiani:** Conceptualization, Writing – review & editing. **Matteo Errigo:** Conceptualization, Writing – review & editing. **Massimiliano Materazzi:** Writing – review & editing, Supervision, Project administration, Funding acquisition.

Declaration of Competing Interest

The authors declare that they have no known competing financial interests or personal relationships that could have appeared to influence the work reported in this paper.

Data availability

Data will be made available on request.

Acknowledgment

The authors wish to acknowledge Professor Pier Ugo Foscolo for the meaningful discussions and comments that greatly improved the quality of the manuscript. The authors also thank UK Research and Innovation (UKRI) for funding this research project.

References

[1] Hofbauer H, Materazzi M. Waste gasification processes for SNG production. Substit Nat Gas from Waste, Elsevier 2019:105–60. https://doi.org/10.1016/B978-0-12-815554-7.00007-6.
[2] Salatino P, Solimene R. Mixing and segregation in fluidized bed thermochemical conversion of biomass. Powder Technol 2017;316:29–40. https://doi.org/10.1016/j.powtec.2016.11.058.
[3] Martinez Castilla G, Larsson A, Lundberg L, Johnsson F, Pallarès D. A novel experimental method for determining lateral mixing of solids in fluidized beds – Quantification of the splash-zone contribution. Powder Technol 2020;370:96–103. https://doi.org/10.1016/j.powtec.2020.05.036.
[4] Müller D, Plankenbühler T, Karl J. A Methodology for Measuring the Heat Release Efficiency in Bubbling Fluidised Bed Combustors. Energies 2020;13:2420. https://doi.org/10.3390/en13102420.
[5] Suárez-Almeida M, Gómez-Barea A, Pfeifer C, Leckner B. Fluid dynamic analysis of dual fluidized bed gasifier for solar applications. Powder Technol 2021;390:482–95. https://doi.org/10.1016/j.powtec.2021.05.032.
[6] Amaya-Santos G, Chari S, Sebastiani A, Grimaldi F, Lettieri P, Materazzi M. Biohydrogen: A life cycle assessment and comparison with alternative low-carbon production routes in UK. J Clean Prod 2021;319:128886. https://doi.org/10.1016/j.jclepro.2021.128886.
[7] Iannello S, Morrin S, Materazzi M. Fluidised bed reactors for the thermochemical conversion of biomass and waste†. Kona Powder Part J 2020;37:114–31. https://doi.org/10.14356/kona.2020016.
[8] Mema I, Buist KA, Padding JT. Fluidization of spherical versus elongated particles : Experimental investigation using magnetic particle tracking 2020:1–13. https://doi.org/10.1002/aic.16895.
[9] Mema I, Padding JT. Spherical versus elongated particles – Numerical investigation of mixing characteristics in a gas fluidized bed. Chem Eng Sci X 2020;8:100079. https://doi.org/10.1016/j.cesx.2020.100079.
[10] Bai Y, Si H. Experimental study on fluidization, mixing and separation characteristics of binary mixtures of particles in a cold fluidized bed for biomass fast pyrolysis. Chem Eng Process – Process Intensif 2020;153:107936. https://doi.org/10.1016/j.cep.2020.107936.
[11] Wang L-J, Wei G-C, Duan S-P, Hou Q-F. CFD-DEM study on the mixing characteristics of binary particle systems in a fluidized bed of refuse-derived fuel. Part Sci Technol 2019;37:51–9. https://doi.org/10.1080/02726351.2017.1338320.
[12] Szücs B, Szentannai P. Experimental Investigation on Mixing and Segregation Behavior of Oxygen Carrier and Biomass Particle in Fluidized Bed. Period Polytech Mech Eng 2019;63:188–94. https://doi.org/10.3311/PPme.13764.
[13] Urciuolo M, Solimene R, Ammendola P, Krusch S, Scherer V, Salatino P, et al. On the agglomeration tendency of carbonaceous fuels in fluidized beds. Fuel 2020;277:118187. https://doi.org/10.1016/j.fuel.2020.118187.
[14] Bruni G, Solimene R, Marzocchella A, Salatino P, Yates JG, Lettieri P, et al. Self-segregation of high-volatile fuel particles during devolatilization in a fluidized bed reactor. Powder Technol 2002;128:11–21. https://doi.org/10.1016/S0032-5910(02)00149-3.
[15] Fiorentino M, Marzocchella A, Salatino P. Segregation of fuel particles and volatile matter during devolatilization in a fluidized bed reactor – II. Experimental. Chem Eng Sci 1997;52:1909–22. https://doi.org/10.1016/S0009-2509(97)00019-5.
[16] Fiorentino M, Marzocchella A, Salatino P. Segregation of fuel particles and volatile matter during devolatilization in a fluidized bed reactor – I Model development. Chem Eng Sci 1997;52:1893–908. https://doi.org/10.1016/S0009-2509(97)00018-3.
[17] Rees AC, Davidson JF, Dennis JS, Hayhurst AN. The rise of buoyant fuel-particles in a slugging gas-fluidized combustor. Chem Eng Res Des 2006;84:319–27. https://doi.org/10.1205/cherd05043.
[18] Solimene R, Marzocchella A, Salatino P. Hydrodynamic interaction between a coarse gas-emitting particle and a gas fluidized bed of finer solids. Powder Technol 2003;133:79–90. https://doi.org/10.1016/S0032-5910(03)00080-9.
[19] Jaya Bharathi. J. KS. Hydrodynamics and Particle Mixing Characteristics of a Ternary Mixture in a Gas-Solid Fluidized Bed. Int J Recent Technol Eng 2019;8:2520–6. https://doi.org/10.35940/ijrte.D7120.118419.
[20] Alagha MS, Szucs B, Szentannai P. Numerical study of mixing and heat transfer of SRF particles in a bubbling fluidized bed. J Therm Anal Calorim 2020;142:1087–96. https://doi.org/10.1007/s10973-019-09135-2.
[21] Köhler A, Rasch A, Pallarès D, Johnsson F. Experimental characterization of axial fuel mixing in fluidized beds by magnetic particle tracking. Powder Technol 2017;316:492–9. https://doi.org/10.1016/j.powtec.2016.12.093.
[22] Köhler A, Pallarès D, Johnsson F. Magnetic tracking of a fuel particle in a fluid-dynamically down-scaled fluidised bed. Fuel Process Technol 2017;162:147–56. https://doi.org/10.1016/j.fuproc.2017.03.018.
[23] Yoshimori W, Ikegai T, Uemoto K, Narita S, Harada S, Oshitani J. Non - invasive measurement of floating – sinking motion of a large object in a gas – solid fluidized bed. Granul Matter 2019;21:1–11. https://doi.org/10.1007/s10035-019-0897-3.
[24] Köhler A, Cano-pleite E, Soria-verdugo A, Pallar D. Modeling the motion of fuel particles in a fluidized bed. Fuel 2021:305. https://doi.org/10.1016/j.fuel.2021.121424.
[25] Soria-Verdugo A, Garcia-Gutierrez LM, Sanchez-Delgado S, Ruiz-Rivas U. Circulation of an object immersed in a bubbling fluidized bed. Chem Eng Sci 2011;66:78–87. https://doi.org/10.1016/j.ces.2010.10.006.
[26] Soria-Verdugo A, Garcia-Gutierrez LM, García-Hernando N, Ruiz-Rivas U. Buoyancy effects on objects moving in a bubbling fluidized bed. Chem Eng Sci 2011;66:2833–41. https://doi.org/10.1016/j.ces.2011.03.055.
[27] Cluet B, Mauviel G, Rogaume Y, Authier O, Delebarre A. Segregation of wood particles in a bubbling fluidized bed. Fuel Process Technol 2015;133:80–8. https://doi.org/10.1016/j.fuproc.2014.12.045.
[28] Stein M, Ding YL, Seville JPK, Parker DJ. Solids motion in bubbling gas fluidized beds. Chem Eng Sci 2000;55:5291–300. https://doi.org/10.1016/S0009-2509(00)00177-9.
[29] Wong YS, Seville JPK. Single-Particle Motion and Heat Transfer in Fluidized Beds 2006;52:4099–109. https://doi.org/10.1002/aic.

[30] Fotovat F, Chaouki J. Characterization of the upward motion of an object immersed in a bubbling fluidized bed of fine particles. Chem Eng J 2015;280:26–35. https://doi.org/10.1016/j.cej.2015.05.130.
[31] Fotovat F, Ansart R, Hemati M, Simonin O, Chaouki J. Sand-assisted fluidization of large cylindrical and spherical biomass particles: Experiments and simulation. Chem Eng Sci 2015;126:543–59. https://doi.org/10.1016/j.ces.2014.12.022.
[32] Köhler A, Pallarès D, Johnsson F. Modeling Axial Mixing of Fuel Particles in the Dense Region of a Fluidized Bed. Energy Fuel 2020. https://doi.org/10.1021/acs.energyfuels.9b04194.
[33] Essenhigh RH, Misra MK, Shaw DW. Ignition of Coal Particles: A Review 1989;30:3–30.
[34] Ponzio A, Sivalingam S, Weihong Y, Wlodzmierz B, Ola E. Ignition of single coal particles in high-temperature oxidizers with various oxygen concentrations 2008;87:974–87. https://doi.org/10.1016/j.fuel.2007.06.027.
[35] Bu C, Leckner B, Chen X, Pallarès D, Liu D, Gómez-Barea A. Devolatilization of a single fuel particle in a fluidized bed under oxy-combustion conditions. Part A: Experimental results. Combust Flame 2015;162:797–808. https://doi.org/10.1016/j.combustflame.2014.08.015.
[36] Iannello S, Foscolo PU, Materazzi M. Investigation of single particle devolatilization in fluidized bed reactors by X-ray imaging techniques. Chem Eng J 2022;431:133807. https://doi.org/10.1016/j.cej.2021.133807.
[37] Jand N, Foscolo PU. Decomposition of wood particles in fluidized beds. Ind Eng Chem Res 2005;44:5079–89. https://doi.org/10.1021/ie040170a.
[38] Scala F. Fluidized Bed Technologies for Near-Zero Emission Combustion and Gasification. 2013. https://doi.org/10.1533/9780857098801.frontmatter.
[39] Hayhurst AN, Parmar MS. Does solid carbon burn in oxygen to give the gaseous intermediate CO or produce CO2 directly? Some experiments in a hot bed of sand fluidized by air. Chem Eng Sci 1998;53:427–38. https://doi.org/10.1016/S0009-2509(97)00334-5.
[40] Hayhurst AN, Parmar MS. Measurement of the Mass Transfer Coefficient and Sherwood Number for Carbon Spheres Burning in a Bubbling Fluidized Bed. Combust Flame 2002;130:361–75.
[41] Kuipers JAM, Prins W, van Swaaij WPM. Theoretical and Experimental Bubble Formation at a Single Orifice in a Two-dimensional Gas-fluidized Bed. Chem Eng Sci 1991;46:2881–94.
[42] Iannello S, Macrì D, Materazzi M. A comprehensive assessment of endogenous bubbles properties in fluidized bed reactors via X-ray imaging. Powder Technol 2023;413:118013. https://doi.org/10.1016/j.powtec.2022.118013.
[43] Gilliland ER. Fluidised particles, J. F. Davidson and D. Harrison, Cambridge University Press, New York(1963). 155 pages.$6.50. AIChE J 1964;10:783–5. https://doi.org/10.1002/aic.690100503.
[44] Kunii D, Levenspiel O. Fluidization Engineering (Second Edition). Fluid Eng 1991;1:1–13. https://doi.org/10.1016/B978-0-08-050664-7.50007-X.
[45] Sebastiani A, Macrì D, Gallucci K, Materazzi M. Steam – oxygen gasification of refuse derived fuel in fluidized beds: Modelling and pilot plant testing. Fuel Process Technol 2021;216:106783. https://doi.org/10.1016/j.fuproc.2021.106783.
[46] Rowe PN, Nienow AW. Particle mixing and segregation in gas fluidised beds. A review. Powder Technol 1976;15:141–7. https://doi.org/10.1016/0032-5910(76)80042-3.
[47] Zhu HL, Zhang YS, Materazzi M, Aranda G, Brett DJL, Shearing PR, et al. Co-gasification of beech-wood and polyethylene in a fluidized-bed reactor. Fuel Process Technol 2019;190:29–37. https://doi.org/10.1016/j.fuproc.2019.03.010.
[48] Rabacal M, Costa M, Vascellari M, Hasse C. Kinetic modelling of sawdust and beech wood pyrolysis in drop tube reactors using advanced predictive models. Chem Eng Trans 2014;37:79–84. https://doi.org/10.3303/CET1437014.
[49] Guizani C, Jeguirim M, Valin S, Limousy L, Salvador S. Biomass chars: The effects of pyrolysis conditions on their morphology, structure, chemical properties and reactivity. Energies 2017;10. https://doi.org/10.3390/en10060796.
[50] Boruvka V, Zeidler A, Holecek T, Dudík R. Elastic and Strength Properties of Heat-Treated Beech and Birch Wood. Forests 2018:1–18. https://doi.org/10.3390/f9040197.
[51] Lisowski A, Matkowski P, Dąbrowska M, Piątek M, Świętochowski A, Klonowski J, et al. Particle Size Distribution and Physicochemical Properties of Pellets Made of Straw, Hay, and Their Blends 2020:63–75. https://doi.org/10.1007/s12649-018-0458-8.
[52] Rezaei H, Panah FY, Lim CJ, Sokhansanj S. Pelletization of refuse-derived fuel with varying compositions of plastic, paper, organic and wood. Sustain 2020;12:1–11. https://doi.org/10.3390/su12114645.
[53] Macrì D, Poletto M, Barletta D, Lettieri P. An investigation of the fl ow properties of rutile particles : Fluidization behaviour linked with shearing studies 2020;374:544–59. https://doi.org/10.1016/j.powtec.2020.07.082.
[54] Dennis JS, Hayhurst AN, Mackley IG. The ignition and combustion of propane/air mixtures in a fluidised bed. Symp Combust 1982;19:1205–12. https://doi.org/10.1016/S0082-0784(82)80297-X.
[55] Vaart DR van der. Freeboard ignition of premixed hydrocarbon gas in a fluidized bed 1988;67:1003–7.
[56] Hesketh RP, Davidson JF. Combustion of Methane and Propane in an Incipiently Fluidized Bed 1991;467:449–67.
[57] Hayhurst AN, Tucker RF. The Combustion of Carbon Monoxide in a Two-Zone Fluidized Bed 1990;189:175–89.
[58] Rees AC, Davidson JF, Dennis JS, Hayhurst AN. The rise of a buoyant sphere in a gas-fluidized bed. Chem Eng Sci 2005;60:1143–53. https://doi.org/10.1016/j.ces.2004.09.045.
[59] Cooke RB, Goodson MJ, Hayhurst AN. The combustion of solid wastes as studied in a fluidized bed. Process Saf Environ Prot Trans Inst Chem Eng Part B 2003;81:156–65. https://doi.org/10.1205/095758203765639852.
[60] Scala F. Fluidized bed technologies for near-zero emission combustion and gasification. n.d.
[61] Arena U, Chirone R, Salatino P. The fate of fixed carbon during the fluidized-bed combustion of a coal and two waste-derived fuels. Symp Combust 1996;26:3243–51. https://doi.org/10.1016/S0082-0784(96)80170-6.